Thermo-mechanical processing of steel: effect on microstructure, crystallographic texture and charpy impact transition behaviour

A. Ghosh, A. Chatterjee, D. Chakrabarti

The severity of fissure formation during Charpy impact testing of low-carbon steel increased with the decrease in finish rolling temperature (820°C - 650°C). Fissure crack develops on the main fracture plane due to the strain incompatibility between cube (ND || <001>) and gamma (ND || <111>) texture bands, which resulted from intercritical rolling. Clustering of ferrite grains having cube texture promotes the subsequent crack propagation along the transverse 'fissure plane'.

KEYWORDS: THERMO-MECHANICAL PROCESSING - LOW-CARBON STEEL - FINISH ROLLING TEMPERATURE - CRYSTALLOGRAPHIC TEXTURE BANDING - CUBE TEXTURE - GAMMA TEXTURE - CHARPY IMPACT TEST - FISSURES - EFFECTIVE GRAIN SIZE

INTRODUCTION

Over the last three decades thermo-mechanically controlled rolled high strength low alloy steels (HSLA) are widely being used in construction, line pipe, pressure vessel, naval, automotive and defense applications. During the Charpy impact testing of such steel at an intermediate test temperature range of 0°C to -80°C, fissure crack (also known as splitting or delamination) is often found, which propagates through the transverse plane with respect to the main fracture plane [1–4]. In general, fissures are considered to be detrimental as it reduces the impact energy absorption capacity of Charpy specimens machined along T-L (Transverse-Longitudinal) orientation with respect to the rolled plates [1–6].

Several investigations have been carried out to understand the effect of microstructural constituents on the fissure formation in steel [1–3,7–10]. A list of those studies is given in **Table 1**. Compared to the studies on microstructural constituents, fewer studies relating crystallographic texture with fissure formation are available. Bourell et al. [4] mentioned that the presence of cube texture (ND || <001>) can be the primary reason behind the fissure formation based on the assumption that preferential alignment of {001} planes of the crystals parallel to the rolling plane weakens the transverse 'fissure plane'. The objective of the present study is to understand the effect of texture on the mechanism of fissure formation in steel.

A. Ghosh, A. Chatterjee, D. Chakrabarti
Department of Metallurgical and Materials Engineering,
I.I.T. Kharagpur, 721302, India.

Corresponding author contact details:
E-mail: debalay@gmail.com;
Phone: +91-9733776579; Fax: +91-3222-282280.

Tab. 1 - Various reasons mentioned in the literature behind the formation of fissure during Charpy impact testing.

Cause behind formation of fissure	Material	Mode of failure	Reference
Elongated ferrite grain structure	Low carbon ferrite pearlite steel, Nb- Zr alloy	Intergranular	[3,5,9,11,12]
High dislocation density within ferrite grains	Low carbon ferrite pearlite steel	Intergranular	[10]
High amount of Sulfur and Phosporus	Dual phase steel	Intergranular	[1,10,13]
Cube fiber texture	Low carbon ferrite pearlite steel	Transgranular / Intergranular	[4,14]
Presence of coarse ferrite grain patches in between the matrix of fine ferrite grains	Low carbon ferrite pearlite steel	Transgranular	[15]
Ferrite pearlite banded microstructure	HSLA steel	Intergranular	[1,2,8]
Through thickness texture band and cube texture cluster on fissure plane	Low carbon ferrite pearlite steel	Intergranular on main fracture plane, Transgranular cleavage on fissure plane	present study

EXPERIMENTAL DETAILS

Samples from a low carbon steel containing 0.1 C, 0.15 Si, 1.25 Mn, 0.01 S, 0.01 P, 0.06 Nb, 0.01 Ti and 0.007 N (wt.%) were soaked at 1200°C for half an hour and rolled down to 15 mm thickness plates in a laboratory rolling mill at finish rolling temperatures of 820°C (Sample code: FRT820), 730°C (Sample code: FRT730) and 650°C (Sample code: FRT650). The amount of intercritical deformation (true strain) applied below the A_{r3} temperature of the steel is 0.0, 0.4, and 0.9 for FRT820, FRT730 and FRT650 samples, respectively. Charpy V-notch specimens were fabricated from the rolled plates along the Transverse-Longitudinal (T-L) orientation following ASTM E-23 standard, and tested in an Instron® 400J impact testing machine (Model: SI-1C3) at -40°C. Electron backscattered diffraction analysis, EBSD, was carried out using a Oxford HKL Channel 5 system attached to Zeiss Auriga Compact SEM at a step size of 1.0 µm and 0.3 µm for low magnification scan and high magnification scan, respectively. EBSD scanning on the fissure crack has been carried out for more than 5 mm crack length for each sample and the length over which the crack is propagating through gamma (ND || <111>) and cube (ND || <001>) interface is carefully measured.

RESULTS AND DISCUSSION

Fissure formation was negligible in FRT820 and the severity of fissure formation increased with the decrease in finish rolling temperature, becoming most severe in FRT650, **Fig. 1(a-c)**. FRT650 and FRT730 showed an average of 3.3 ± 0.5 and 1.2 ± 0.4 number of fissures per tested sample, respectively. The RD-ND plane is the 'main fracture plane' and the fissure crack propagates along the transverse RD-TD plane, which is termed as 'fissure plane', **Fig. 1(d)**. The presence of micro-voids on the main fracture plane indicate to the occurrence of ductile fracture, **Fig. 1(e)**. However, cleavage facets, indicating brittle fracture, have been found inside the splits, i.e. on the fissure plane, **Fig. 1(f)**.

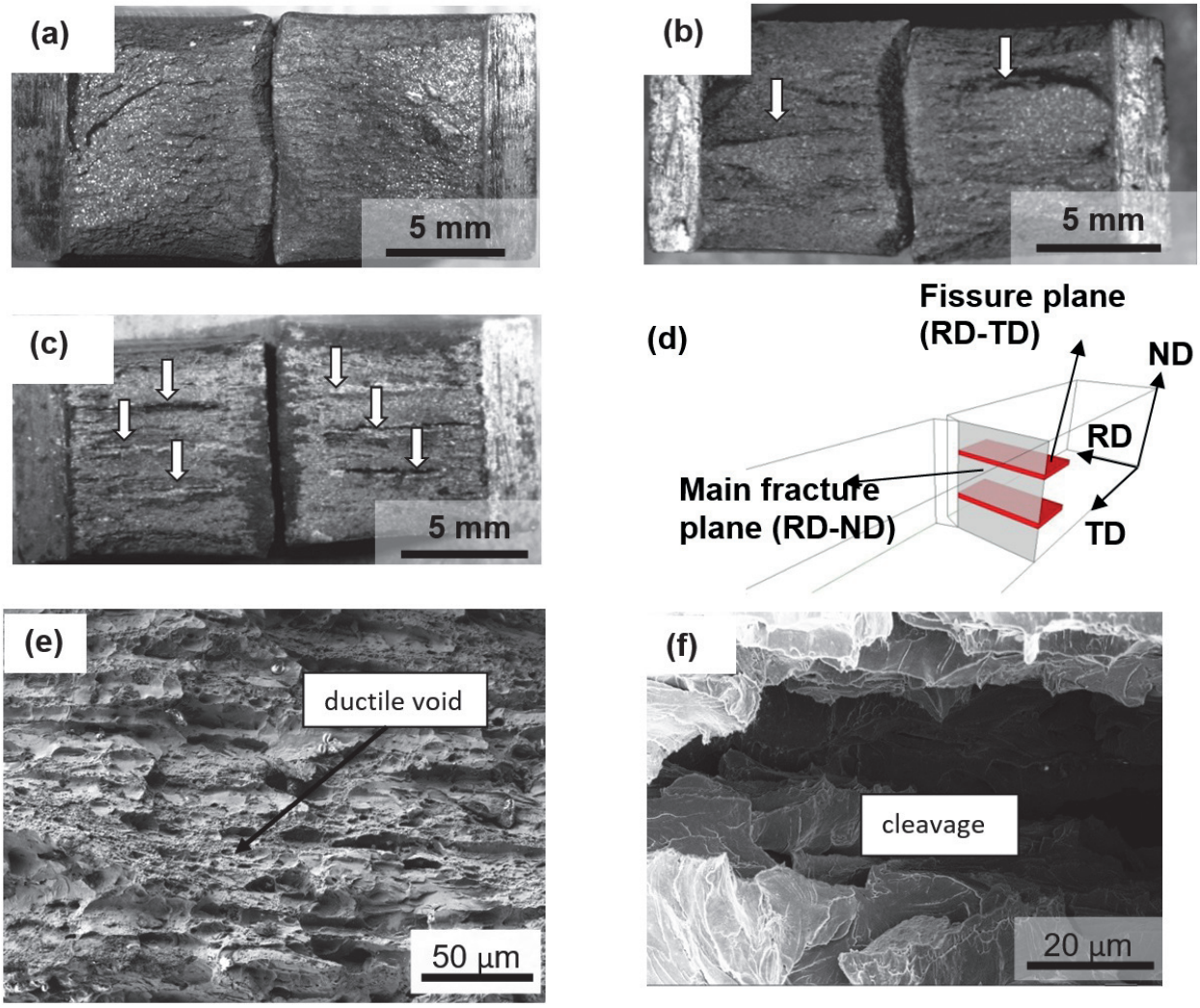

Fig. 1 - (a-c) Macro-view on the fracture surfaces of the Charpy impact samples of (a) FRT820 (b) FRT730, and (c) FRT650; (d) Schematic diagram showing the main fracture plane (Grey color) and fissure plane (Red color) in a Charpy sample; (e, f) SEM fractographs of FRT650 showing (e) ductile voids on the main fracture plane and (f) cleavage facets on the fissure plane.

Optical micrographs of the investigated samples show the ferrite-pearlite microstructure with pearlite content lying in close range (12-14%). EBSD analysis revealed the presence of a through thickness texture band comprising of cube and gamma texture components on the main fracture plane of FRT73 and FRT650, as shown in **Fig. 2 (b and c)**, respectively. On the other hand, no texture banding has been found in FRT820, and the texture was more random, **Fig. 2a**. The banding is found to be stronger in FRT650 (average band length 25.0 ± 12.1 µm, average band width 8.6 ± 4.3 µm) as compared to FRT730 (average band length 16.8 ± 5.1 µm, average band width 10.7 ± 3.2 µm).

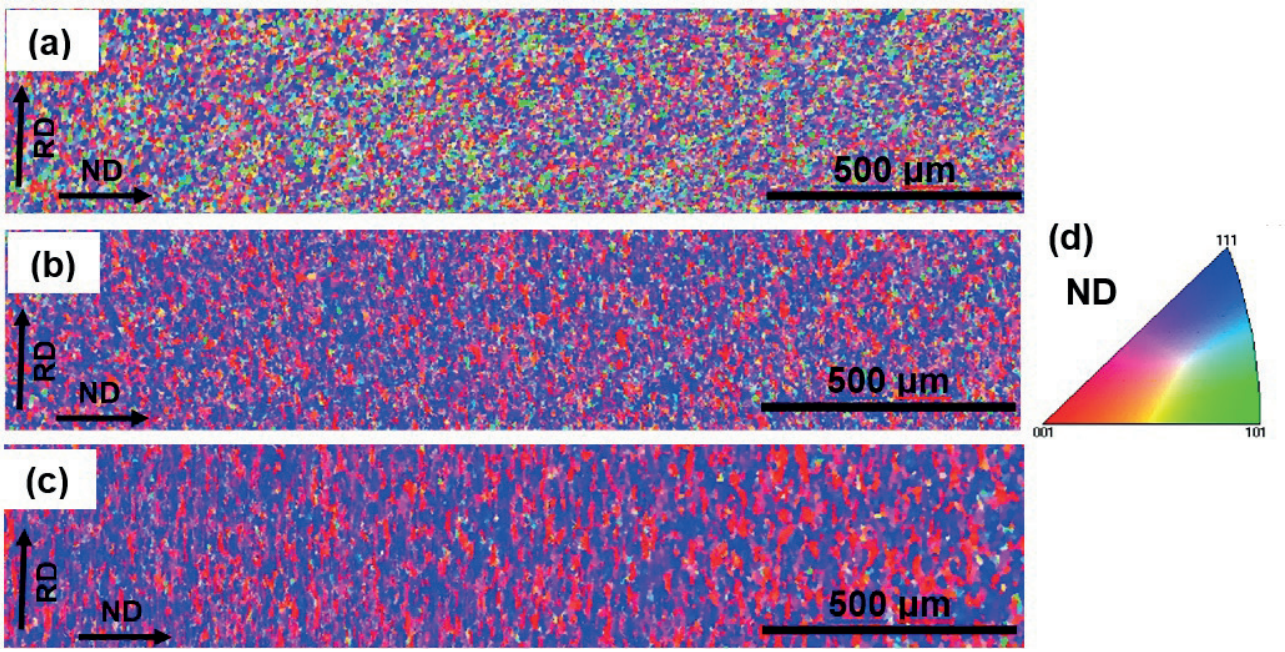

Fig. 2 - Inverse pole figure (IPF) map on the main fracture plane of (a) FRT820, (b) FRT730 and (c) FRT650; the color legend is given in (d). Cube texture and gamma texture are represented by 'red' and 'blue' colour, respectively.

In order to identify the origin of fissures, a thin layer of the metal has been removed from the fracture surface until sufficient depth can be reached so that fissure cracks become very fine and the crack propagation through the microstructure can be studied. EBSD analysis on that plane reveals that the fissure crack propagates on the main fracture plane predominantly (~75% - 80% cases) through the interface of gamma and cube texture components as indicated by arrows in **Fig. 3a**. The SEM micrograph in **Fig. 3b** indicated that the fissure crack propagation occurred through the interface between severely deformed and lightly deformed ferrite grains. The local average misorientation angle was measured and found to be higher within the gamma component (2.3°) compared to that within the cube component (1.6°) in FRT650. In case of deformation under plane strain compression and considering slip occurs only on the {110}<111> slip system, the Taylor factor was calculated for all possible orientations of a ferrite crystal as presented in ϕ_2=45° section of the Eulers' space in **Fig. 3c**. Due to the higher Taylor factor, gamma texture component (>3.2) is expected to posses higher dislocation density as compared to cube texture component (<2.2), and therefore, a strain incompatibility can arises in-between gamma and cube oriented grains [16] during the deformation of the sample. That is why, a difference in the matrix strain and local average misorientation has been noticed at both sides of the fissure crack, **Fig. 3b**. Although the fissure crack may initiate from ferrite-pearlite interface or from the inclusions [1,2,8,10,13], as per the present observation the fissures propagate in an ductile fashion through the interface between severely deformed and lightly deformed ferrite grains having two different crystallographic orientations, on the main fracture plane.

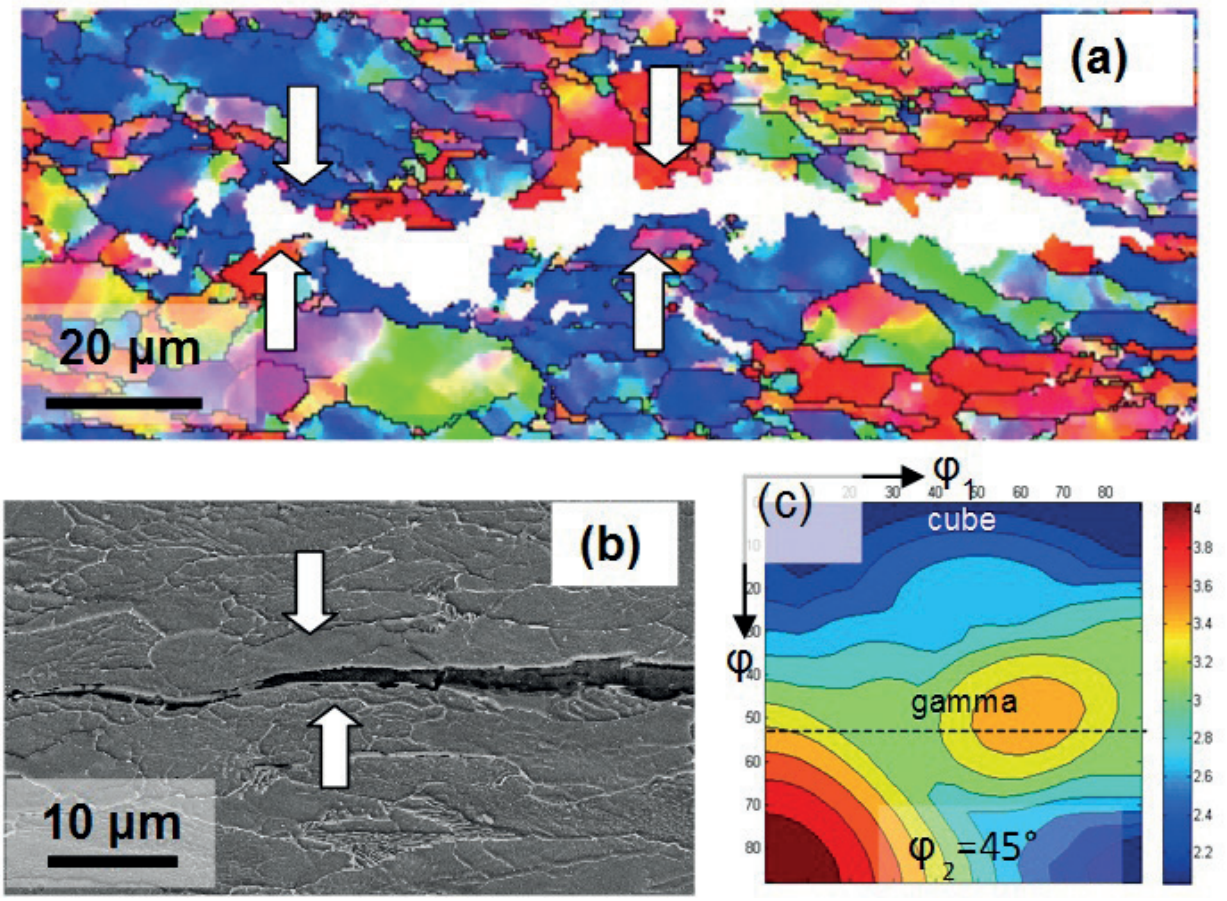

Fig. 3 - (a) Inverse pole figure (IPF) map of the region surrounding a hairline fissure crack on RD-ND plane (parallel to main fracture plane). Colour legend is given in Fig. 2d; (b) SEM image showing the propagation of fissure crack through the deformed and undeformed grains; (c) Taylor factor map for different crystallographic orientations represented within the ϕ_2=45° section of Eulers space.

Now, cube and gamma texture banding on main fracture plane can cause different coherent length of {001} planes on the fissure plane, perpendicular to main fracture plane, at two different texture layers. The cluster of cube oriented grains (in red colour) has been found to be frequently interleaved on the fissure plane of FRT650 as indicated by the dotted circle in **Fig. 4a**. Average cube cluster sizes in FRT730 and FRT650 samples are 40 ± 12 µm and 72 ± 16 µm, respectively. Such a cluster of cube textured grains may form due to the extended recovery of initially transformed proeutectoid ferrite, which was subjected to intercritical deformation [17]. The IPF map in **Fig. 4a** shows the presence of high angle grain boundaries (black lines) within a cluster of cube oriented grains. Although, the grain boundary misorientation angle in between the adjacent ferrite grains (both having cube orientation) is higher than 15°, the angle between the {001} planes of those grains is low (<5°). The schematic diagram in **Fig. 4b** explains this aspect further, where the exact orientation of the adjacent crystals within a cube cluster is shown.

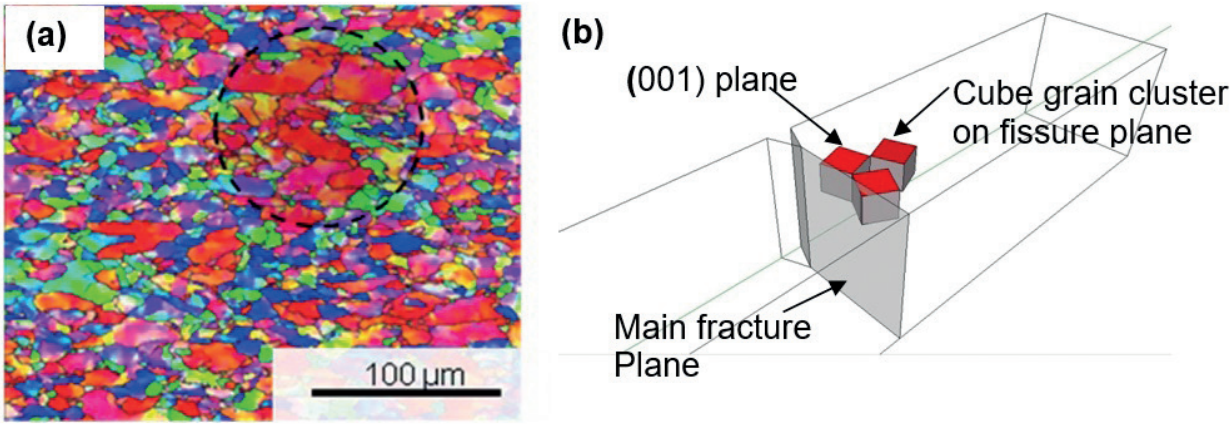

Fig. 4 - (a) Inverse pole figure (IPF) map on fissure plane (RD-TD) of FRT650. Colour legend is given in Fig. 2d; (b) Schematic showing the clustering of cube oriented grains on the fissure plane.

Cleavage fracture along the transverse fissure plane (RD-TD) is energetically difficult as the normal stress acting on the main fracture plane ($2.18\sigma_y$) is expected to be 1.3 times higher than the normal stress acting on the fissure plane ($1.68\sigma_y$) under plane strain condition at the general yielding temperature (where, σ_y is the yield stress) [4]. In spite of having the above mentioned constraint, the cleavage fracture can still occur on the fissure plane rather than the main fracture plane provided the cleavage fracture stress of the fissure plane (σ_{ff}) is sufficiently lower than the cleavage fracture stress on the main fracture plane (σ_{fm}). As per the present hypothesis the criterion for fissure formation can be given by the following equation:

$$\sigma_{fm} \geq 1.3 \times \sigma_{ff} \quad (1)$$

In our recent work [18], it has been shown that the cleavage crack deviation at the grain boundary depends on the angle between {001} planes of the crystals rather than their misorientation angle. Following this approach 15° misorientation threshold between the {001} planes of the neighbouring crystals is considered to estimate, the effective grain size, on the fissure plane as well as on the main fracture plane, **Table 2**. Due to higher cube texture clustering the average value of effective grain size on the fissure plane (RD-TD) is found to be significantly higher in FRT650, compared to FRT730 and FRT820, **Table 2**. In case of FRT650, the effective grain size on the fissure plane is ~2 times of the effective grain size estimated on the main fracture plane by considering the proposed threshold criterion, **Table 2**.

The cleavage fracture stress (σ_f) can be related to the average ferrite grain size (d) of the steel using Griffith equation modified by Orowan [19], as given below:

$$\sigma_f = \sqrt{\frac{2E\gamma_{eff}}{\pi d}} \quad (2)$$

where, γ_{eff} represents the effective plastic work and E is the elastic modulus. The cleavage fracture stress on the main fracture plane and fissure plane can be calculated by taking constant value of γ_{eff} (52 J/m^2) and E (210 GPa) as reported in literature [20, 21], **Table 2**.

Tab. 2 - Effective grain size and cleavage fracture stress on RD-ND and RD-TD planes of the investigated samples.

Sample name	Plane	Effective grain size considering {001} cleavage plane (µm)	Cleavage fracture stress (MPa)	Ratio
FRT820	Main fracture plane (RD-ND)	13.8±0.5	710	0.96
	Fissure Plane (RD-TD)	12.8±0.2	737	
FRT730	Main fracture plane (RD-ND)	20.4±2.8	584	1.27
	Fissure Plane (RD-TD)	32.8±4.9	460	
FRT650	Main fracture plane (RD-ND)	32.6±2.3	462	1.38
	Fissure Plane (RD-TD)	62.4±9.6	334	

In FRT650, the cleavage fracture stress on the main fracture plane is 1.38 times of that on the fissure plane, resulting in cleavage crack propagation along the fissure plane, in spite of higher normal stress acting on the main fracture plane. In case of FRT730, the σ_{ff} to σ_{fm} ratio (~1.27) is close to the condition mentioned in **eqn. 1**. As a result, intermediate fissure formation has been observed in that sample. In case of FRT820 the σ_{ff} to σ_{fm} ratio (~0.96) is well below the threshold value (1.3), leading to the absence of fissure.

CONCLUSIONS

In summary, the fissure crack propagates in ductile fashion on the main fracture plane (RD-ND) along the interface of cube and gamma texture bands due to the strain incompatibility. Eventually the fissure crack propagates in transgranular cleavage mode along the fissure plane aided by the clustering of cube oriented grains, which promotes cleavage crack propagation by increasing, the effective grain size, and reducing the cleavage fracture stress on that plane. The, effective grain, size estimated from the threshold criterion based on the angle between {001} planes of the neighbouring crystals can explain the weakness of the fissure plane. The severity of fissure formation was found to be directly related to the difference in cleavage fracture stress between the 'main fracture plane' and the 'fissure plane'.

ACKNOWLEDGEMENTS

Financial support from Department of Science and Technology (DST), New Delhi, and the experimental support from FIB-EBSD-SEM laboratory, C.R.F., IIT Kharagpur, are duly acknowledged. Sincere thanks to the Administration of Indian Institute of Technology Kharagpur for permitting Dr. DC to visit Italy and present the paper in TMP 2016 Conference.

REFERENCES

[1] E.A. ALMOND, Metall. Trans. A 1, (1970), p. 2038.
[2] H. HERø, J. EVENSEN, J.D. EMBURY, Can. Metall. Q. 14, (1975), p. 117.
[3] B.L. BRAMFITT, A.R. MARDER, Metall. Trans. A 8, (1977), p. 1263.
[4] D.L. BOURELL, Metall. Trans. A 14, (1983), p. 2487.
[5] B. MINTZ, E.M. MAINA, W.B. MORRISON, Mater. Sci. Technol. 24, (2008), p. 177.
[6] M. JOO, D. SUH, J. BAE, H. BHADESHIA, Mater. Sci. Eng. A 546, (2012), p. 314.
[7] M. YANG, Y.J. CHAO, X. LI, J. TAN, Mater. Sci. Eng. A 497, (2008), p. 451.
[8] M. YANG, Y.J. CHAO, X. LI, D. IMMEL, J. TAN, Mater. Sci. Eng. A 497, (2008), p. 462.
[9] B. MINTZ, E. MAINA, W.B. MORRISON, Mater. Sci. Technol. 23 (2007), p. 347.
[10] B. MINTZ, W.B. MORRISON, Mater. Sci. Technol. 4, (1988), p. 719.
[11] S.M. TOKER, F. RUBITSCHEK, T. NIENDORF, D. CANADINC, H.J. MAIER, Scr. Mater. 66, (2012), p. 435.
[12] Y. KIMURA, T. INOUE, F. YIN, K. TSUZAKI, Science 320, (2008), p. 1057.
[13] M. YANG, Y.J. CHAO, X. LI, J. TAN, Mater. Sci. Eng. A 497, (2008), p. 451.
[14] R. SCHOFIELD, G. ROWNTREE, N. V. SARMA, R.T. WEINER, Met. Technol. 1, (1974), p. 325.
[15] R. PUNCH, M. STRANGWOOD, C. DAVIS, Metall. Mater. Trans. A 43, (2012), p. 4622.
[16] A. ARSENLIS, D. PARKA, Acta Mater. 47, (1999), p. 1597.
[17] R.D. DOHERTY, D.A. HUGHES, F.J. HUMPHREYS, J.J. JONAS, D.J. JENSEN, M.E. KASSNER, W.E. KING, T.R. McNELLEY, H.J. McQUEEN, A.D. ROLLETT, Mater. Sci. Eng. A 238, (1997), p. 219.
[18] A. GHOSH, S. KUNDU, D. CHAKRABARTI, Scr. Mater. 81, (2014), p. 8.
[19] D. BROEK, Elementary Engineering Fracture Mechanics, Springer Netherlands, Dordrecht, (1986).
[20] J.H. CHEN, L. ZHU, H. MA, Acta Metall. Mater. 38, (1990), p. 2527.
[21] J.M. SAN MARTIN, J.I., RODRIGUEZ-IBABE, Scr. Mater. 40, (1999), p. 459.